

# Modeling the Performance of a Photovoltaic Cell based on Crystalline Silicon

Bouzaki Mohammed  
Moustafa  
URMER Research unit,  
Tlemcen University  
BP. 119, Tlemcen, Algeria

Benyoucef Boumediene  
URMER Research unit,  
Tlemcen University  
BP. 119, Tlemcen, Algeria

Soufi Aicha  
URMER Research unit,  
Tlemcen University  
BP. 119, Tlemcen, Algeria

Mamar Hichem  
URMER Research unit,  
Tlemcen University  
BP. 119, Tlemcen, Algeria

Chadel Meriem  
URMER Research unit,  
Tlemcen University  
BP. 119, Tlemcen, Algeria

## ABSTRACT

The doping concentration and the thickness of crystalline silicon solar cells strongly influence their performances. In this work we simulated a solar cell with ZnO/c-Si(n)/c-Si(p)/c-Si(p)/Ag structure. The optimization of thicknesses and doping concentrations of the emitter, absorber and the BSF layers were performed using the AFORS-HET simulation software.

## General Terms

Simulation, AFORS-HET, performance, crystalline silicon solar cell

## Keywords

Simulation, AFORS-HET, performance, crystalline silicon solar cell

## 1. INTRODUCTION

High purity silicon wafers are the most widespread material to produce solar cells. However, an elegant alternative and actual extension lies in the thin-film technology [1]. The thin-film solar cells could very well reduce the cost of photovoltaic (PV) cells to a potentially lower cost than the “traditional” silicon wafer solar cells. This technology reduces also the amount of silicon used, and hence the cost per watt of power output, and allows for the use of poorer-quality materials to achieve a given efficiency.[2,3,4,5,6]

The present market situation, however, reflects a completely different reality: over 90% of sold PV are based on crystalline silicon wafers or ribbon material. One of the reasons for the lower manufacturing cost of wafer solar cells is the higher conversion efficiency potential of a crystalline silicon solar cell.[7]

Crystalline silicon is an indirect band-gap semiconductor, i.e. its near-band-gap absorption is phonon-assisted, with a band-gap of 1.12 eV at a cell temperature equal to 300 K [8]. It have the advantages of market dominance, non-toxicity, abundance, stability, high efficiency potential and the ability to share research and infrastructure costs with the integrated circuit industry [2,3].

Silicon is one of the most studied elements in the periodic table, and silicon technology is by far the most advanced among all semiconductor technologies. When a semiconductor is doped with impurities, the semiconductor becomes extrinsic and impurity energy levels are introduced. When a boron atom with three valence electrons substitutes for a silicon atom, an additional electron is accepted to form four covalent bonds around the boron, and a positively charged hole is created in the valence band. This is p-type semiconductor, and boron is an acceptor. If a pentavalent impurity atom such as phosphorus is substituted into the diamond lattice in place of a host atom, there will be one valence electron from the impurity atom left over after the four covalent bonds are formed with the nearest neighbors. An impurity atom that results in an excess electron is referred to as a donor. Semiconductors in which electrons are the dominant carriers are called n-type semiconductors.[9]

Numerical simulation is very important for the design and understanding of solar cells. AFORS-HET (Automat For Simulation of HETero-structures) has been developed by a group from the Hahn-Meitner Institute of Berlin. It is used in simulating hetero-junction in solar cells [10] and provides a convenient way to evaluate the role of the various parameters present in the fabrication process [11,12].

In this paper, with the purpose of reducing the cost furthermore and promoting the performances of crystalline silicon solar cells, we optimize the doping concentrations and the thicknesses of the different layers of the solar cell.

## 2. SOLAR CELL STRUCTURE AND SIMULATION DETAILS

We simulated the solar cell structure ZnO/c-Si(n)/c-Si(p)/c-Si(p)/Ag as shown in Fig.1. The cells consist of the c-Si(n) emitter layer, the c-Si(p) absorber layer and the c-Si(p) BSF layer. The front and back contacts were assumed to be flat bands in order to neglect the contact potential influence.

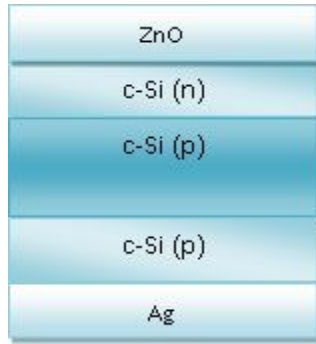


Fig 1: Schematic structure of the simulated solar cell

The surface recombination velocities of electrons and holes were both set as  $10^7$  cm/s. The solar AM1.5 radiation was adopted as the illuminating source with a power density of  $100\text{mW/cm}^2$ .

Beside this, various other standard layers parameters are taken into consideration in the simulation. The used values are given in table 1.

Table 1. Parameter values adopted for the solar cell in the simulation

| Parameter   | c-Si (n)              | c-Si (p)              | c-Si (p)              |
|---|-----------------------|-----------------------|-----------------------|
| Thickness (nm)  | 500                   | 300.000               | 500                   |
| Dielectric constant   | 11,9                  | 11,9                  | 11,9                  |
| Electron affinity (eV)  | 4,05                  | 4,05                  | 4,05                  |
| Band gap (eV)   | 1,12                  | 1,12                  | 1,12                  |
| Effective conduction band density ( $\text{cm}^{-3}$ )                        | $2,8 \times 10^{19}$  | $2,8 \times 10^{19}$  | $2,8 \times 10^{19}$  |
| Effective valence band density ( $\text{cm}^{-3}$ )                           | $1,04 \times 10^{19}$ | $1,04 \times 10^{19}$ | $1,04 \times 10^{19}$ |
| Electron mobility ( $\text{cm}^2\text{V}^{-1}\text{s}^{-1}$ )                 | 1040                  | 1040                  | 1040                  |
| Hole mobility ( $\text{cm}^2\text{V}^{-1}\text{s}^{-1}$ )                     | 412                   | 412                   | 412                   |
| Doping concentration of acceptors ( $\text{cm}^{-3}$ )                        | 0                     | $1 \times 10^{16}$    | $1 \times 10^{19}$    |
| Doping concentration of donators ( $\text{cm}^{-3}$ )                         | $1 \times 10^{19}$    | 0                     | 0                     |
| Thermal velocity of electrons ( $\text{cm s}^{-1}$ )                          | $10^7$                | $10^7$                | $10^7$                |
| Thermal velocity of holes ( $\text{cm s}^{-1}$ )                              | $10^7$                | $10^7$                | $10^7$                |
| Layer density ( $\text{g cm}^{-3}$ )  | 2,328                 | 2,328                 | 2,328                 |
| Auger recombination coefficient for electron ( $\text{cm}^6 \text{s}^{-1}$ )  | $2,2 \times 10^{-31}$ | $2,2 \times 10^{-31}$ | $2,2 \times 10^{-31}$ |
| Auger recombination coefficient for hole ( $\text{cm}^6 \text{s}^{-1}$ )      | $9,9 \times 10^{-32}$ | $9,9 \times 10^{-32}$ | $9,9 \times 10^{-32}$ |
| Direct band-to-band recombination coefficient ( $\text{cm}^3 \text{s}^{-1}$ ) | $1,1 \times 10^{-14}$ | $1,1 \times 10^{-14}$ | $1,1 \times 10^{-14}$ |

### 3. RESULTS AND DISCUSSION

#### 3.1 Optimization of thickness of different layers

The dependence of some of the cell parameters on the thickness of the emitter layer is shown in Fig.2. It is seen that when increasing the emitter layer thickness from 10 nm to 80 nm, The output voltage ( $V_{oc}$ ) has increased from 628,90 mV to 630,46 mV. However, beyond an emitter layer thickness of 80 nm, it is found that the output voltage decreases continuously. The lowest  $V_{oc}$  value of 625,78 mV is obtained for a thickness of 1000 nm. The figures also show that the  $J_{sc}$  variable drops from  $37,64 \text{ mA/cm}^2$  to  $29,68 \text{ mA/cm}^2$  when continuously increasing the emitter thickness from 10 nm to 1000 nm. This reduction of  $J_{sc}$  is accompanied by an enhancement in losses of absorption at the emitter layer surface. The parameter FF decreases, initially, from 78,04% to 77,87% when varying the emitter thickness from 10 nm to 80 nm. However, starting from a thickness of 80 nm and up to 1000 nm, this parameter increases continuously from 77,87 % to 78,36 %. The efficiency  $\eta$  is found to drop from 18,47% to 14,55% when changing the emitter layer thickness from 10 nm to 1000 nm.

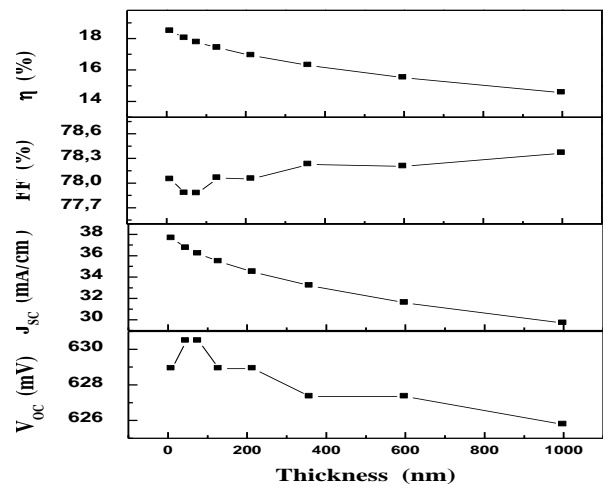


Fig2: Effects of the thickness of emitter layer (c-Si (n)) on the performance of the solar cell.

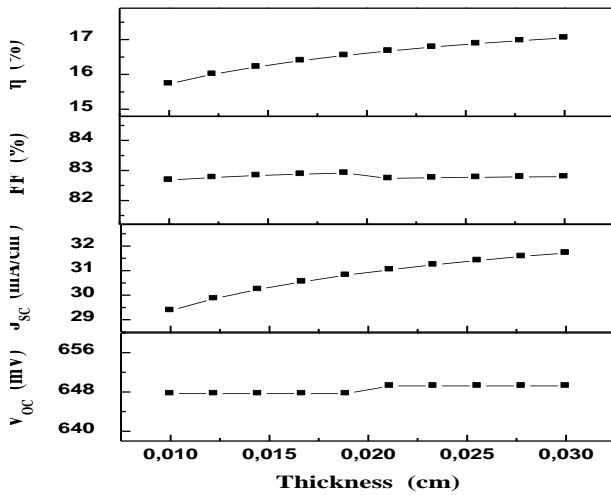


Fig 3: Effects of the thickness of absorber layer (c-Si (p)) on the performance of the solar cell.

The dependence of the variables  $V_{OC}$ ,  $J_{SC}$ , FF and  $\eta$  on the thickness of the absorber layer is shown in Fig.3. According to this figure,  $J_{SC}$  and  $\eta$  increase almost linearly as the thickness of the c-Si base is increased from 100  $\mu\text{m}$  to 300  $\mu\text{m}$ . FF, in contrast, shows only a weak sensitivity to the absorber thickness. Values as high as 649,21 mV, 31,71 mA/cm<sup>2</sup> and 17,04%, are obtained for  $V_{oc}$ ,  $J_{sc}$  and  $\eta$ , respectively. They correspond to a thickness of the c-Si base of 300  $\mu\text{m}$ . The observed enhancement of  $J_{sc}$  at high thicknesses is ascribed to an increase in the generation of e-h pairs. This increase in the e-h pair creation also explains the  $\eta$  behavior.

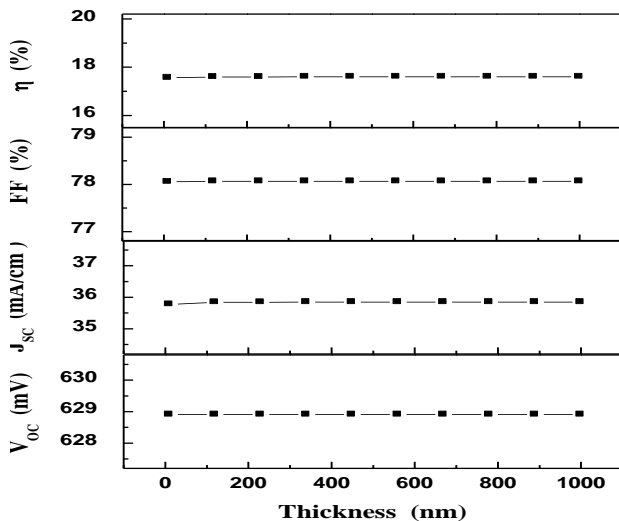


Fig4: Effects of the thickness of BSF layer (c-Si (p)) on the performance of the solar cell.

Figure 4 shows that the four studied variables show no sign of dependence on the range of thicknesses of the BSF layer we have considered in the simulation. We accordingly fix the thickness of this layer at 300 nm.

### 3.2 Optimization the doping concentration of different layers

Figure 5 illustrates the effect of the a-Si:H(n) layer doping concentration on the performance of the solar cell. We can see that there is a very sharp increase of the variables  $V_{oc}$ , FF and  $\eta$  at the beginning of the studied range of the concentration. However, above a certain value of  $3 \times 10^{20} \text{ cm}^{-3}$  the values of  $V_{OC}$ , FF and  $\eta$  reach saturation, and therefore we can choose  $3 \times 10^{20} \text{ cm}^{-3}$  as optimal concentration. We should note that a larger acceptors concentration than this value is difficult to realize in the laboratory.

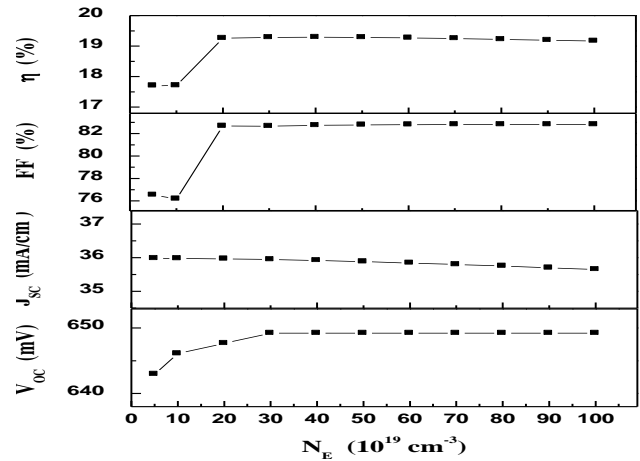


Fig 5: Effects of doping concentration of the emitter layer c-Si (n) on the performance of the solar cell.

The effects of the c-Si (p) doping concentration on the performance of the solar cell are shown in Fig.6. The results indicate that the doping concentration influences  $V_{OC}$ ,  $J_{SC}$ , FF and  $\eta$  only at quite small values. Hence, it can be considered that a concentration of  $5 \times 10^{15} \text{ cm}^{-3}$  can be quite representative of acceptable doping concentrations.

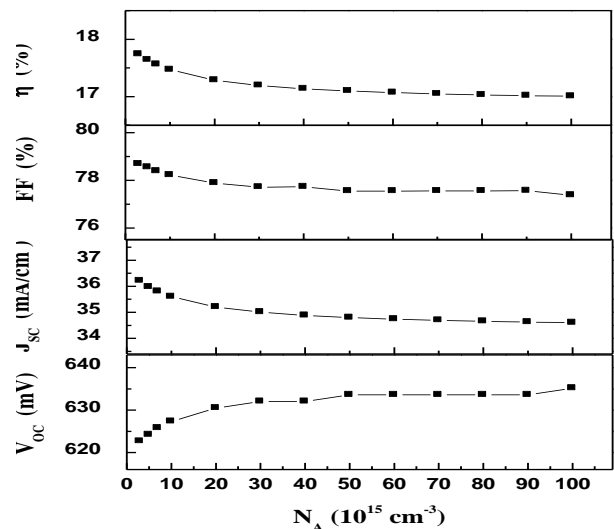


Fig 6: Effects of doping concentration of absorber layer c-Si (p) on the performance of the solar cell.

Back surface field (BSF) is an effective way to enhance the performance of crystalline silicon solar cells. As seen from the

Fig.7, when doping concentration of BSF layer increases, the performance of the solar cell also increases ( $V_{OC}$ : 649,21 ~ 699,21 mV;  $J_{SC}$ : 35,94 ~ 36,55 mA; FF: 82,65 ~ 82,92 %;  $\eta$ : ~ 21,19 %). But when the doping concentration is higher than  $1 \times 10^{20} \text{ cm}^{-3}$ , the performances parameters of the solar cell remain constant.

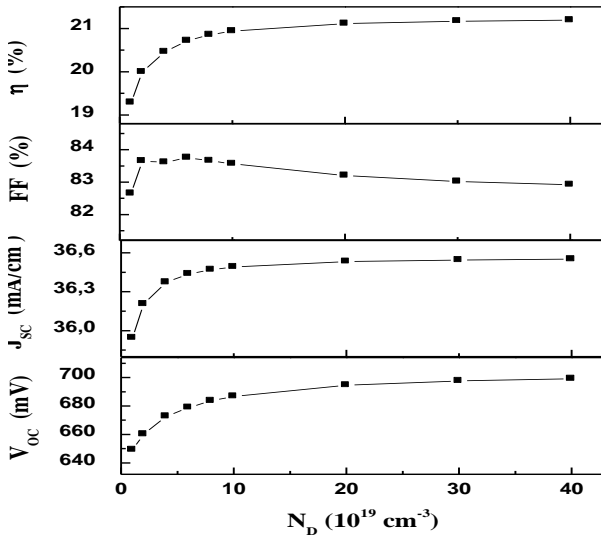


Fig 7: Effects of doping concentration of BSF layer c-Si (p) on the performance of the solar cell.

#### 4. CONCLUSION

The effects of the doping concentration and the thickness of different layers on the performances of crystalline silicon solar cells are studied using AFORS-HET simulation software. Optimizing the performance parameters we realized a record efficiency of 21,11%,  $V_{OC}$  of 69,45mV,  $J_{SC}$  of 36,53mA/cm<sup>2</sup> and FF of 83,20% . These values were obtained at thicknesses of 100nm, 300 $\mu$ m and 300nm of the emitter, the absorber and the BSF layers, respectively. The doping concentrations were fixed at  $3 \times 10^{20} \text{ cm}^{-3}$ ,  $5 \times 10^{15} \text{ cm}^{-3}$  and  $2 \times 10^{20} \text{ cm}^{-3}$  for the emitter, the absorber and the BSF layers.

#### 5. ACKNOWLEDGMENTS

The authors wish to thank Helmholtz-Zentrum Berlin for providing the AFORS-HET simulation software. A free copy can be downloaded from [http://www.helmholtzberlin.de/forschung/enma/sipv/projekte/asicsi/afors-het/index\\_en.html](http://www.helmholtzberlin.de/forschung/enma/sipv/projekte/asicsi/afors-het/index_en.html).

#### 6. REFERENCES

[1] T. Kunz a,n, V.Gazuz a, M.T.Hessmann a, N.Gawehns a, I.Burkert a, C.J.Brabec a,b “Laser structuring of

crystalline silicon thin-film solar cells on opaque foreign substrates “ Solar Energy Materials & Solar Cells 95 (2011) 2454–2458

- [2] Kylie R. Catchpole, Michelle J. McCann, Klaus J. Weber, Andrew W. Blakers “A review of thin film crystalline silicon for solar cell applications. Part 2: Foreign substrates” Solar Energy Materials & Solar Cells 68 (2001) 173}215
- [3] C.S.Solanki a, R.R.Bilyalov a, J.Poortmans a, G.Beaucarne a, K.V an Nieuwenhuysena, J.Nijls b, R.Mertens a,b “Characterization of free-standing thin crystalline films on porous silicon for solar cells” Thin Solid Films 451 –452 (2004) 649–654
- [4] Philipp Rosenits , Fabian Kopp, Stefan Reber “Epitaxially grown crystalline silicon thin-film solar cells reaching 16.5% efficiency with basic cell process” Thin Solid Films 519 (2011) 3288–3290
- [5] Michelle J. McCann\*, Kylie R. Catchpole, Klaus J. Weber, Andrew W. Blakers “A review of thin-”lm crystalline silicon for solar cell applications. Part 1: Native substrates” Solar Energy Materials & Solar Cells 68 (2001) 135-171
- [6] J. Poortmans, V. Arkhipov “Thin Film Crystalline Silicon Solar Cells on low Cost Silicon Carriers” Thin Film Solar Cells (2006)
- [7] Stefan Reber, Achim Eyer, Fridolin HAAS “High-throughput zone-melting recrystallization for crystalline silicon thin-film solar cells” Journal of Crystal Growth 287 (2006) 391–396
- [8] Leo J.H. Lin a, Y.-P. Chiou a,b “Improving thin-film crystalline silicon solar cell efficiency with back surface field layer and blaze diffractive grating” Solar Energy 86 (2012) 1485–1490
- [9] JongHoe Wang “Resistivity distribution of silicon single crystals using codoping” Journal of Crystal Growth 280 (2005) 408–412
- [10] Arturo Morales-Acevedo, Norberto Hernández-Como, Gaspar Casados-Cruz “Modeling solar cells: A method for improving their efficiency” Materials Science and Engineering B 177 (2012) 1430– 1435.
- [11] Norberto Hernandez-Como, Arturo Morales-Acevedo “Simulation of heterojunction silicon solar cells with AMPS-1D” Solar Energy Materials & Solar Cells 94 (2010) 62–67.
- [12] LIU Qin, YE Xiao-jun, LIU Cheng, and CHEN Ming-bo “Performance of bifacial HIT solar cells on n-type silicon substrates” Optoelectronics LETTERS VOL.6 No.2, 1 March 2010.